AIAA JOURNAL
Vol. 34, No. 3, March 1996

Atomic Oxygen Line Shape Measurement at 130 nm with Raman-Shifted Laser

Scott A. Meyer*
Stanford University, Stanford, California 94305-4035
Surendra P. Sharma†
NASA Ames Research Center, Moffett Field, California 94035-1000
Daniel Bershader‡
Stanford University, Stanford, California 94305-4035
Ellis E. Whiting§
Thermophysics Institute, Moffett Field, California 94035-1000
Richard J. Exberger¶
NASA Ames Research Center, Moffett Field, California 94035-1000
and
John O. Gilmore**
Stanford University, Stanford, California 94305-4035

The absorption of vacuum ultraviolet light by atomic oxygen has been measured in the electric arc-driven shock tube facility at NASA Ames Research Center. A probe beam is generated with a Raman-shifted ArF excimer laser. By suitable tuning of the laser, absorption is measured over a range of wavelengths in the region of the $^3P_1$-$^3S^0$ line at 130.49 nm. The Lorentzian full width at half-height due to collision broadening by atomic oxygen is measured at various wavelengths up to 1200 linewidths away from the line center. The measured linewidth is three times larger than that calculated with an established radiation code, and a possible explanation for the difference is discussed. This experiment demonstrates the viability of high-order Raman shifters as light sources in impulse facilities where singnal averaging is not possible.

Introduction

SHAPES of spectral lines can play an important role in radiative transfer by lines with large transition probabilities, such as the prominent oxygen triplet near 130 nm. Measurement of absorption at this transition is a candidate for an atomic oxygen concentration diagnostic. The lower level is the electronic ground state, and so the amount of absorption can be easily related to the number of oxygen atoms. However, the line shape must be known to deduce the number of atoms from the measured absorption at a given frequency. Also, the line shape for this transition is of more general interest because of its importance of radiative transport. Atomic line emission can potentially lead to very high radiative heating of hypervelocity vehicles in planetary atmospheres, but the actual heat load depends on the amount of self-absorption in these lines. Accurate calculations, in both of the cases mentioned, requires detailed knowledge of the line shape in the wings.

Shapes of spectral lines have been studied for many years, and mathematical expressions have been derived to describe them.[1-3] The most commonly used line shape is the Voigt profile, which is a convolution of Gaussian and Lorentzian components and is symmetrical about the line center. The Gaussian component is produced by the Doppler effect, a result of the random thermal motion of the atoms or molecules. The Lorentzian component results from approximations that describe the effects of collisions with other particles and by internal quantum mechanical effects. Gaussian and Lorentzian profiles are conveniently characterized by their linewidth, that is, the full width of the line at half of the maximum intensity. A Voigt profile requires two parameters, such as the widths of the Gaussian and Lorentzian components.

Accuracy of theoretical predictions beyond about one linewidth from the line center is still uncertain because of the limited data on collisional broadening. The region near the line center is often known reasonably well, because this region is usually dominated by the Gaussian component. However, the Gaussian decays very quickly and is virtually absent beyond three linewidths from the line center. The Lorentzian component decays much more slowly than the Gaussian component and provides the major contribution to the expressions for the line shape in the wings. The Lorentzian profile is also most accurate near the line center, whereas in the line wings many of the approximations used to derive it are highly questionable.

Unfortunately, few data exist to evaluate the accuracy of the theory in the wings. Measurements of broadening due to collisions are most frequently reported for collisions with gas species other than the absorbing species. In the present study we are interested in self-broadening, which is broadening due to collisions with the same specie. Self-broadening measurements have generally been made in atomic gases such as hydrogen, noble gases, alkalis, and a few other metallic vapors.[4] However, the valence state of oxygen is very different from these species because its ground state is split into three sublevels. Experimental measurements of the broadening of atomic oxygen allow an assessment of this effect on the collisional broadening theory.

This paper describes a line shape measurement of the atomic oxygen line at 130.49 nm. The experiment requires a narrowband, tunable source of vacuum ultraviolet (VUV) light and a well-defined source of atomic oxygen. Previous studies of VUV absorption have relied on various types of discharge lamps, which produced continuum or line radiation.[5] Line sources emit at discrete, fixed

Presented as Paper 95-0290 at the AIAA 33rd Aerospace Sciences Meeting, Reno, NV, Jan. 9–12, 1995; received Feb. 14, 1995; revision received Sept. 8, 1995; accepted for publication Sept. 15, 1995.

*Graduate Student, Department of Aeronautics and Astronautics. Student Member AIAA.
†Senior Research Scientist. Associate Fellow AIAA.
‡Professor, Department of Aeronautics and Astronautics (deceased).
§Research Fellow.
¶Research Associate.
**Graduate Student, Department of Mechanical Engineering. Student Member AIAA.

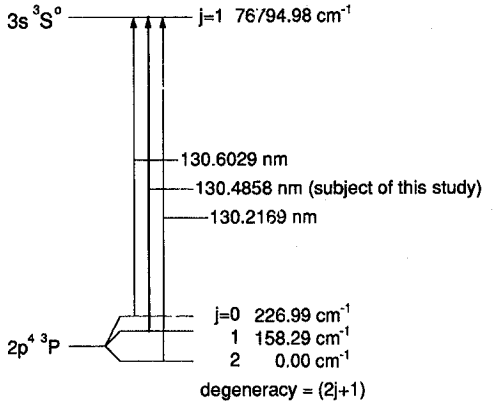

Fig. 1 Partial energy level diagram for atomic oxygen showing the VUV absorption transitions near 130 nm.

wavelengths, whereas continuum sources are generally too weak for shock tube measurements. We circumvent these limitations with a tunable excimer laser whose wavelength is shifted to overlap with the VUV absorption line. Atomic oxygen is generated in a shock tube by dissociating pure O_2 at conditions that assure thermodynamic equilibrium. The dissociated test gas must be free of any significant amount of O_2 or other absorbing species that would interfere with the measurement. Composition and temperature of the test gas are determined from the one-dimensional Rankine–Hugoniot relations. Thus, the absorption produced by a known number of oxygen atoms is measured at various locations from near the line center to 1200 Lorentzian linewidths into the wings.

Theory—Atomic Oxygen Absorption

The ground state of atomic oxygen is a ^3P state, as shown in Fig. 1. This state is split into three closely spaced j levels ($j = 0$, 1, and 2) by spin-orbit coupling, and the degeneracy of each level is $(2j + 1)$. At room temperature, most of the atoms are in the $j = 2$ level. As the temperature increases, the relative populations of the j levels approach the ratio of the degeneracies, i.e., 1:3:5. The relative population ratio is 1:3:1:5.3 at the nominal temperature of 6100 K achieved here, which is very close to the high temperature limit. The wavelengths of the $^3P_{0,1,2} \rightarrow {}^3S^0$ lines are 130.6029, 130.4858, and 130.2169 nm.[6] In units of frequency (or photon energy), the line positions are 76567.99, 76636.69, and 76794.98 cm^{-1}. [While some spectroscopic identifications and regions are identified by wavelength units (nm), lineshape results are presented in terms of photon frequency ($1/\lambda$, cm^{-1}). For reference, a width of 1 cm^{-1} = 0.017 nm at 76637 cm^{-1}.] Observation at high resolution reveals the spectral widths of these lines.

The line shape function is used in Beer's law to calculate transmission at a given frequency:

$$I(\bar{\nu})/I_0(\bar{\nu}) = \exp[-NL\sigma_0\phi(\bar{\nu})] \tag{1}$$

where frequency is in cm^{-1}, ϕ is in cm^{-1}, N is in cm^{-3}, σ_0 is in cm^{-1}-cm^2, and L is in cm. The frequency dependence is contained in the line shape function ϕ. The path length L is a measurable quantity, and the frequency-integrated absorption cross section σ_0 is calculated from the spontaneous transition probability per particle per second, A_{ul}, which is assumed to be known for a given transition.[7] The line shape function is determined empirically by measuring the fraction of the beam that is transmitted, I/I_0, through a known number density of atomic oxygen over a range of VUV laser frequencies.

Radiative transfer calculations facilitate analysis of our measurements. First, test conditions in the shock tube are verified by comparing intensity-calibrated emission spectra to synthesized spectra. Then, having determined the composition and temperature of the gas, we compare the VUV absorption measurements to calculated absorption profiles. Both types of calculations are performed with the NEQAIR5 code. Details of the spectral line shape models are described here, and more general information about the code is found in the Appendix.

The theoretical line shape function in NEQAIR5 is based on several well-known approximations.[2] It is modeled with a Voigt profile whose Gaussian linewidth is determined by Doppler broadening. The Lorentzian linewidth is a sum of the natural and collisional linewidths. Expressions in NEQAIR5 for linewidths from the various broadening mechanisms are reproduced in Eqs. (2–5). The Doppler linewidth is given by

$$\Delta\bar{\nu} = 7.16 \times 10^{-7}\bar{\nu}\sqrt{(T/M)} \tag{2}$$

where T is the translational temperature in degrees Kelvin and $M = 16$ for atomic oxygen. The natural linewidth is calculated from the lifetimes of the upper and lower levels for the transition and is given by

$$\Delta\bar{\nu} = 5.309 \times 10^{-12}[(1/\tau_u)] + (1/\tau_l)] \tag{3}$$

where τ is in seconds. For the lines near 130 nm, $\tau_u = 1.57 \times 10^{-9}$ s,[8] and $\tau_l \gg 1$ s.[9]

Contributions to the collisional linewidth are calculated for collisions with electrons, similar atoms, and other gas species present. The expression for calculating the linewidth for electron broadening is given by

$$\Delta\bar{\nu} = 2 \times 10^{-16}\gamma N_e(T/10000\,\mathrm{K})^{0.38} \tag{4}$$

where N_e is the number density of electrons in cm^{-3}. For the lines near 130 nm, $\gamma = 0.046$ cm^{-1}-cm^3.

Collisions with other oxygen atoms are the dominant broadening mechanism in the present study, and this self-broadening is given by

$$\Delta\bar{\nu} = \frac{1.03 \times 10^{-13}A_{ul}N_l}{(\bar{\nu})^3}\sqrt{(g_u/g_l)} \tag{5}$$

where N_l is the number density of potential collision partners in cm^{-3} and g_u and g_l are the degeneracies of the upper and lower levels, respectively.

Collision broadening is a complicated process, and Eq. (5) is derived from an approximate model described in Ref. 10. The model is derived for the shape of an emission line generated by a radiating atom, i.e., the reverse of the absorption process in the present case. The leading term in the interaction potential between the colliding atoms is the dipole-dipole interaction,

$$V_{dd} = \left[\frac{\boldsymbol{d}_r\cdot\boldsymbol{d}_p}{|\boldsymbol{r}|^3} - 3\frac{(\boldsymbol{d}_r\cdot\boldsymbol{r})(\boldsymbol{d}_p\cdot\boldsymbol{r})}{|\boldsymbol{r}|^5}\right] \tag{6}$$

where $\boldsymbol{d}_r$ and $\boldsymbol{d}_p$ are the dipole moment operators of the radiating and perturbing atoms, respectively, and $\boldsymbol{r}$ is the position vector between the perturber and the radiating atom. The only nonvanishing contribution to the linewidth is from resonant energy exchange between the two dipoles, which is accurate to second order in the classical path approximation. Equation (5) is the Lorentzian linewidth given by the impact approximation using V_{dd}. In this approximation, the duration of the collision is much shorter than the time between collisions. This assumption is reasonable near the line center, but it may not be appropriate in the line wings. Ali and Griem[10] also show that higher order terms in the interaction potential, such as the van der Waals term, should have a relatively small effect in the case of resonant energy exchange. At small interatomic distances, the higher order terms can become significant.

The interaction in Eq. (6) arises from a quantum-mechanical resonance that exists between two like atoms. In this process, the two atoms are exchanging virtual photons. This interaction occurs for collisions with atoms in any level that is connected to the excited state by a dipole-allowed transition. In the case of oxygen, transitions from $^3S^0$ to many other levels are dipole-allowed, including the three j levels of the ^3P ground state. Of these levels, however, only the ^3P ground state is appreciably populated at 6100 K. Thus, N_l in Eq. (5) should be the number density of oxygen atoms in the ^3P state, which is nearly equal to the total number density of oxygen atoms. Therefore, the resonance collisional width for all three lines should be the same. However, in NEQAIR5, only oxygen atoms in

Table 1 Shock tube test conditions

Shock speed, Km/s	6.83 − 0.16	6.83	6.83 + 0.16
Temperature, K	5400	6100	6800
Number density of O, cm^{-3}	9.6×10^{17}	9.0×10^{17}	8.4×10^{17}
Number density of O_2, cm^{-3}	6×10^{15}	2×10^{15}	5×10^{14}
Number density of e^-, cm^{-3}	2×10^{13}	7×10^{13}	3×10^{14}

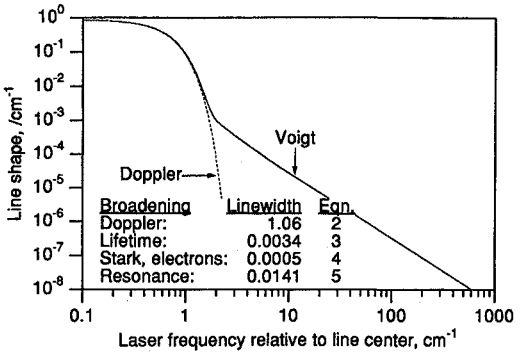

Fig. 2 Calculated line shape function for the nominal test conditions shown in Table 1.

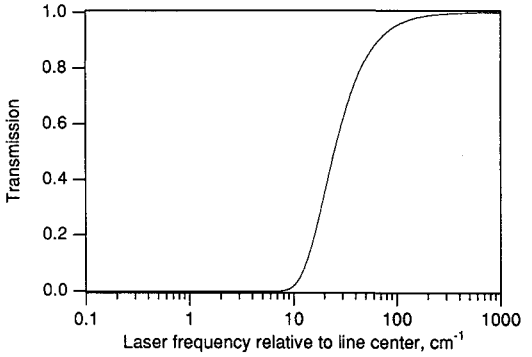

Fig. 3 Calculated transmission through a 10-cm path of atomic oxygen for the conditions of Table 1 and the Voigt profile in Fig. 2.

the same j level, i.e., $^3P_1$ for 130.49 nm, are treated as the collision partners. As implemented in NEQAIR5, N_l for the $j = 1$ line (130.49 nm) is approximately one-third of the atomic oxygen number density, and the relative collisional widths of the three lines are proportional to the populations in the absorbing levels.

The line shape of the $j = 1$ atomic oxygen line calculated with NEQAIR5 is plotted in Fig. 2. The calculations are for the nominal test conditions, which are shown in Table 1 and described in the next section. Both scales are logarithmic to illustrate the functional dependence near the line center and in the line wing regions. Doppler broadening, described by the Gaussian profile, is dominant near the line center but decreases rapidly in the line wings. The Lorentzian decays more slowly and becomes the dominant component in the line wing region. The Lorentzian linewidth is determined from both collisional broadening by other oxygen atoms and by the natural linewidth. Note that the calculated value of the resonance linewidth is four times larger than that of the natural linewidth for lifetime broadening and 28 times larger than the Stark linewidth due to electrons.

The transmission calculated for this line shape using Eq. (1) is shown in Fig. 3. Thermodynamic conditions are the same as those in the line shape calculation and the path length is 10 cm, corresponding to the diameter of the shock tube used in the test. Optimal depth at the center of the line, $NL\sigma_0\phi(0)$, exceeds 10^5, so the line is black in this region; the measured transmission is essentially zero. Therefore, useful absorption measurements can only be made by tuning the laser into the line wings, where the line shape is dominated by collisional broadening, as shown in Fig. 2. In this region, spectral resolution requirements are much less stringent than near the center of the line.

Experimental Description

Atomic Oxygen Source

Atomic oxygen is generated in the electric arc-driven shock tube (EAST) facility at NASA Ames Research Center. A diagram of the shock tube and the experimental setup is shown in Fig. 4. The shock tube has an arc-heated driver and an aluminum driven section 10 cm in diameter. A capacitor bank is discharged through the driver gas, producing high temperature and pressure in the driver section.[11] This produces a strong shock wave in the driven section. In this study, the facility generates a shock wave with a nominal speed of 6.8 km/s. The facility must be cleaned and the driver section reassembled after each shot, which limits facility operation to one shot per day.

The shock tube must provide an atomic oxygen sample in thermodynamic equilibrium with a minimum of other species, especially molecular oxygen and free electrons, for this experiment to be effective. Molecular oxygen absorbs at the same wavelengths as atomic oxygen, and significant ionization would make Stark broadening dominate the line shape. Thus, the presence of either O_2 or free electrons in the test gas would complicate the interpretation of the absorption measurements. We calculated equilibrium temperature and species compositions as a function of incident shock speed, shown in Fig. 5, to find conditions that meet these criteria. The target shock speed selected was 6.8 km/s because, as the figure shows, it provides nearly complete dissociation of the O_2 and only a small concentration of electrons. These equilibrium calculations are used later in the data analysis to deduce test conditions from the measured shock speed.

A further restriction on the test condition is the allowable test gas density in the shock tube. Number density must be high enough to achieve a reaction rate that dissociates the O_2 during the available test time. However, if the density is too high, the absorption will be so strong that the three atomic lines will merge into a single spectral feature. The density is chosen low enough to permit meaningful absorption measurements and high enough to provide an adequate dissociation rate. We find that an initial gas pressure in the shock tube of 1 torr meets these experimental requirements.

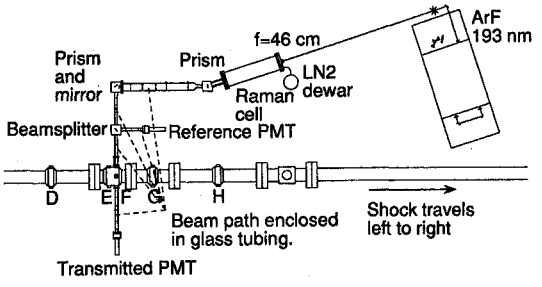

Fig. 4 Layout of VUV absorption instrumentation. The excimer beam is focused into the Raman cell to generate the VUV probe beam. The desired beam is separated from the others with prisms and directed through the shock tube.

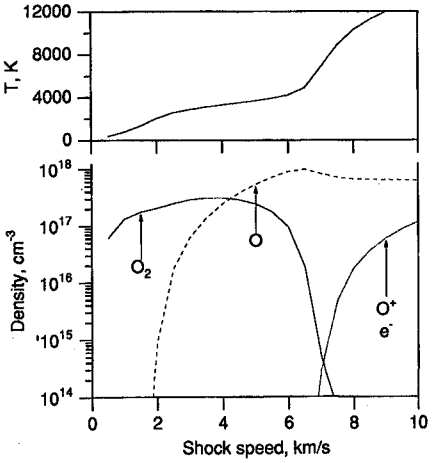

Fig. 5 Calculated conditions behind a shock into 1.0 torr of pure O_2.

Shock propagation is monitored with time-of-arrival measurements using ionization probes and pressure transducers at various stations along the driven tube. Shock speed is deduced from the measurements, and we observe attenuation of the shock. Four possible sources of the attenuation are considered. Viscous effects at the wall lead to growth of a boundary layer, which acts as a sink for shock-heated gas and attenuates the shock. Extensive work on this subject is summarized by Mirels[12] and has subsequently been re-evaluated numerically.[13] In EAST, spatial and temporal nonuniformities in the driver gas can also lead to either acceleration or deceleration of the shock front. Finally, interaction with the expansion fan and finite rate chemistry can also produce attenuation, but neither is important here. A rapid pressure drop behind the shock indicates that the expansion has overtaken the shock and is not observed. Likewise, dissociation is sufficiently rapid that the finite reaction rate affects the nonequilibrium region behind the shock but does not attenuate the shock.

As a result of the observed attenuation, the state of the oxygen passing the test section is a function of time, according to the shock speed at which the gas was shocked and any subsequent processes. Measured shock attenuation is 600 s^{-1}, corresponding to a gradient of equilibrium temperature, dT/dL, of 1700 K/m. The gradient of atomic oxygen number density is 7×10^{16} cm^{-3}/m.

The measured shock speed is corrected for attenuation with the following approximate model. Laboratory time is converted into particle time to determine the upstream location where the gas was shocked, and the shock speed, at that location, is determined from the measured shock attenuation, dU_s/dL,

$$\Delta U_s = \eta t_{\text{lab}} U_s \left(1 - \frac{1}{\eta}\right) \frac{dU_s}{dL} \tag{7}$$

$$U_{\text{effective}} = U_{\text{measured}} + \Delta U_s \tag{8}$$

The shock speed U_s in meters per second and the attenuation dU_s/dL in second^{-1} are measured, and the density ratio across the shock ($\eta = \rho_2/\rho_1$) is calculated from the Rankine–Hugoniot relations. Temperature, pressure, and composition of the test gas are then computed for the effective shock speed, as shown in Fig. 5.

The flow behind the shock wave is monitored with time-resolved emission measurements. A typical trace from a photomultiplier sensitive over 125–165 nm is shown in Fig. 6. This spectral region contains emission from the O_2 Schumann–Runge bands and the atomic O triplet that is the subject of this study. The time resolution of the emission trace is limited to about 1 μs by the width of the shock tube window. The initial spike is due to the nonequilibrium overshoot,[14] which occurs during the dissociation process, and is followed by a quasi-steady-state (QSS) region before the arrival of the driver gas. The gradual increase in the intensity after the nonequilibrium spike is due to the gradual increase in the effective shock speed as given in Eq. (8). The increase in intensity is indicative of only moderate changes in temperature because the excited state populations (and the emission intensity) depend strongly on temperature.

The reacting flow behind the incident shock is calculated with NONEQ[14,15] using chemical reaction rates derived for a two-temperature model. The model equates the rotational temperature to the translational temperature and the free electron kinetic and electronic temperatures to the vibrational temperature. Vibrational relaxation is treated with the modified Landau–Teller model, which limits the relaxation rate to the gas-kinetic collision rate at high temperatures.

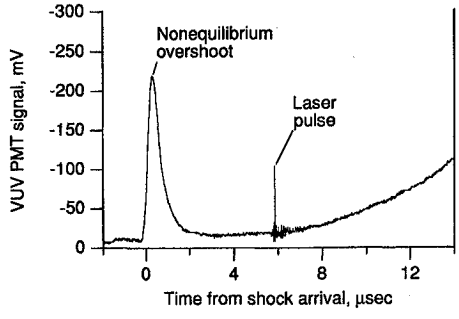

Fig. 6 VUV emission behind the incident shock wave.

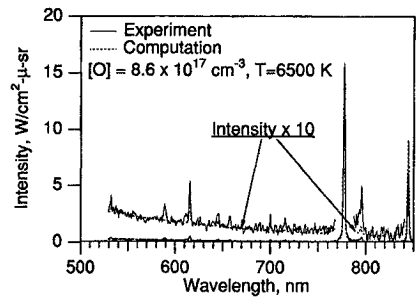

Fig. 7 Comparison of measured and synthetic spectra of test gas. Emission is dominated by atomic oxygen lines. Intensity of some portions of the spectrum are multiplied by a factor of 10 to show weaker lines.

The calculations of the reaction zone length are compared with radiometer measurements. The calculated temperature and composition both reach their equilibrium values within 2 μs of laboratory time after the shock passes. This is consistent with the width of the intensity peak detected behind the shock wave, as shown in Fig. 6.

Characterization of Test Gas

The condition of the test gas, after equilibrium is established, is checked by collecting emission spectra in the range 530–850 nm. Spectra are recorded by focusing an image of the test section onto the entrance slit of a 0.3-m spectrometer with an intensified diode array. A long-pass filter eliminates second-order lines, and a 150 lines/mm grating yields an effective resolution of 1.8 nm. The intensifier acts as a shutter, with a gate width of 2.8 μs, and spectra are collected at various delay times after the shock passes the window. The spectra are calibrated for absolute intensity with a tungsten lamp.

A typical spectrum is shown in Fig. 7. Two portions of the spectrum are also shown with the intensity multiplied by a factor of 10 to illustrate some of the low intensity values. The spectra are all qualitatively similar and consist primarily of atomic oxygen emission lines with a weak background. The 777 ($3s^5S^0$-$3p^5P$) and 845 nm ($3s^3S^0$-$3p^3P$) triplets are most intense, but other OI emission features are also identified at 533 ($3p^5P$-$5d^5D^0$), 616 ($3p^5P$-$4d^5D^0$), 646 ($3p^5P$-$5s^5S^0$), and 700 nm ($3p^3P$-$4d^3D^0$). Although weaker, the latter features are produced by radiation from highly excited levels (>100,000 cm^{-1}), and their intensities are strong functions of temperature.

Atomic emission spectra are synthesized with NEQAIR5 for a uniform, one-dimensional slab; self-absorption in the cooler boundary layer has a negligible effect on emission in this spectral region. The QSS and Boltzmann calculations are virtually identical for all lines except the 777 and 845 nm triplets. Using the QSS approximation, the 777-nm triplet is weaker by a factor of 4–7 than when using the Boltzmann calculation, and the 845-nm triplet weaker by a factor of 2 or less. The difference between the two calculations is likely due to limitations in the present QSS calculation that only includes excitation by electrons. At our test condition, the number of electrons is small (see Fig. 5). Although collisions with heavy particles are less efficient than those with electrons, the frequency of heavy particle collisions is several orders of magnitude higher than that for electrons. The QSS calculation, therefore, represents a lower bound to the line intensities, and the calculation assuming a Boltzmann distribution is in better agreement with the measurements.

Temperature of the test gas is determined by changing the temperature until the calculated line intensities are in agreement with measured absolute intensities. The temperature corresponds to the conditions behind a shock wave of a given speed, as shown in Fig. 5. Thus, the shock speed is deduced from the temperature fit to the measured spectra, with a typical uncertainty of 0.05 km/s.

Shock speeds deduced from the spectra and derived from the shock attenuation measurements are compared in Fig. 8. Effective shock speed is normalized by the incident shock speed and is plotted as a function of time after shock arrival. Horizontal bars on the emission data indicate the gate time during which each spectrum is collected, and so the emission measurements are effectively

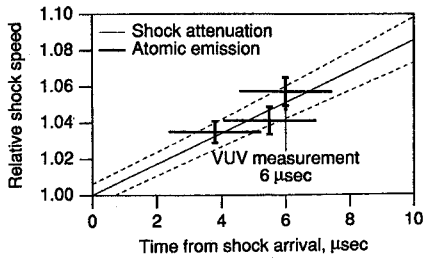

Fig. 8 Comparison of effective shock speed derived from emission spectra to measured shock speed corrected for observed attenuation.

averaged over this time. Agreement between these measurements verifies that the test gas conditions agree well with those predicted by shock speed measurements. As the figure shows, the VUV absorption measurement is made 6 μs after shock passage when the test conditions are known.

Absorption data were collected on 11 shock tube runs, with a mean effective shock speed of 6.83 km/s and a standard deviation of 0.16 km/s. Equilibrium conditions behind the shock wave are calculated with the EQGAS code, which solves the one-dimensional shock wave equations for a real gas. Routines for calculating the thermodynamic properties are extracted from Ref. 16. Partition functions of the atomic and molecular components are computed from tabulated values of spectroscopic constants. For diatomic molecules, the number of bound rotational and vibrational states are determined, and the partition functions are calculated accordingly. The partition function for atomic oxygen includes energy levels up to 108,700 cm^{-1}. Equilibrium compositions are found from the thermodynamic properties derived from the partition functions. Results of the computations are shown in Table 1 for the nominal shock speed and for shock speeds one standard deviation higher and lower than nominal.

VUV Absorption Instrumentation

Absorption by the atomic oxygen line at 130.49 nm is measured with the instrumentation shown in Fig. 4. A pulsed ArF laser generates tunable light at 193 nm. The light is focused into a Raman shifter to produce a series of Stokes and anti-Stokes beams, including the desired wavelength of 130 nm. Efficiency of the conversion to 130 nm is extremely low, and we estimate the energy of the VUV beam is less than 1 μJ in a pulse shorter than 10 ns, but this produces easily measurable transmission signals. Wavelength of the vacuum ultraviolet beam is tuned by adjusting the wavelength of the ArF laser. Several O_2 Schumann–Runge absorption lines overlap the ArF tuning range, and these lines are used for wavelength calibration.[17] In separate measurements, a microwave discharge flow cell produces a continuous source of low-density oxygen atoms. Laser-induced fluorescence excitation scans at 130.49 nm yield a VUV linewidth of 0.9 cm^{-1}, full width at half maximum (FWHM), and an absolute wavelength reference that verifies wavelength calibration with Schumann–Runge absorption. Although the laser linewidth is much larger than the Lorentzian width of the oxygen lineshape, our resolution is sufficient because the measurements are made in the far wings; the Lorentzian width is only a parameter that characterizes the lineshape.

The Raman shifter is a stainless steel cell with windows at each end, filled with hydrogen at 350 torr and at a temperature of 77 K. Linearly polarized beams at several wavelengths are generated in the focal volume, and one of these overlaps the atomic oxygen line at 130.49 nm.[18,19] This beam is separated from the others by a 30-deg MgF_2 prism, and a second prism eliminates stray light. Two photomultipliers measure both the incident and the transmitted intensities. These photomultipliers have KBr photocathodes that are insensitive to any residual light at 193 nm.

Results

Results of the absorption measurements are shown in Fig. 9 as a function of the laser frequency relative to the center of the line at 130.49 nm, corresponding to absorption from the $j = 1$ level. The two shaded areas show the tuning ranges of the laser. The gap in the tuning region is due to absorption of the ArF pump laser

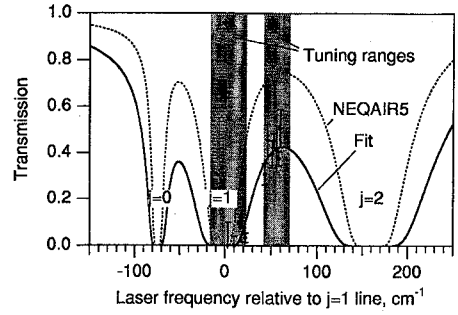

Fig. 9 Measured transmission in the region of atomic oxygen resonance triplet at 130 nm.

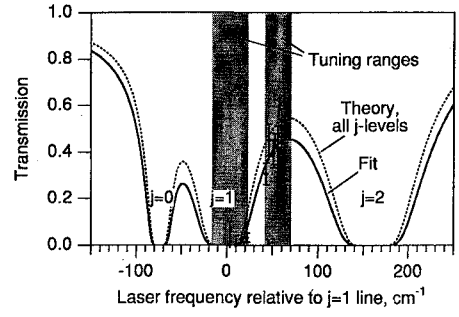

Fig. 10 Comparison of measurements to theory including collisions with ground state oxygen atoms in all three j levels.

by atmospheric O_2 between the laser and the Raman cell. In this spectral region, the laser energy entering the Raman cell is not high enough for Raman shifting to 130 nm.

Measurements in the longer wavelength region show complete attenuation of the beam near the center of the $j = 1$ line, with increasing transmission as the laser is tuned away from the line center. This trend continues in the shorter wavelength region out to about 60 cm^{-1} from the line center, where contributions from the wings of the $j = 2$ line become important. The vertical bars illustrate uncertainties of one standard deviation in the reference intensity I_0. Calibration is performed with the shock tube evacuated before each run to relate the transmitted and reference signals for 100% transmission. With this calibration, I_0 is deduced from the reference signal measured during the run. Scatter in the calibration produces uncertainty in I_0, and measured transmission, for single-shot measurements. The horizontal bars are due to the finite laser bandwidth and uncertainties in the laser frequency calibration. These uncertainties are small relative to the width of the absorption line. The absence of any measurable signal at the line center demonstrates the absence of stray or scattered light in the experiment.

Theoretical and empirical curves are also included in Fig. 9. The theoretical curve is calculated using NEQAIR5 for a gas in equilibrium behind a 6.83 km/s shock. The computation predicts that the three lines of the triplet overlap significantly in the wings. Consequently, complete transmission is not expected between the lines. The measurements show that this expectation is correct.

The empirical curve is fitted by adjusting the Lorentzian linewidth of match the data and to correct for the contribution of the $j = 2$ line. Adjacent components of the triplet must be included because of the contribution in the line wings. The ratio of the linewidths for the three components is held constant to reduce the number of free parameters. The Lorentzian linewidth deduced from the data is 0.053 ± 0.011 cm^{-1} and is measured out to 1200 Lorentzian linewidths from the line center. This experimental linewidth is approximately three times larger than the value of 0.018 cm^{-1} predicted by NEQAIR5.

The measurements are compared with a second set of theoretical and empirical curves in Fig. 10. The theoretical curve is again calculated with NEQAIR5 for the same test conditions. However, in this case the linewidth calculation is modified so that the number of perturbers, N_i in Eq. (5), is the number density in the entire ^3P ground state, which is nearly equal to the total atomic oxygen number density. Therefore, the line broadening calculation for the $j = 1$ line

includes collisions with nearly three times as many atoms. The contribution to the Lorentzian linewidth from resonance broadening, Eq. (5), is increased from 0.014 to 0.044 cm^{-1}. This new theoretical curve, shown in Fig. 10, is in better agreement with the experimental measurements.

The empirical value of the Lorentzian width increases to $0.062 \pm 0.012\ cm^{-1}$ when collisions with all j levels are included because the wings of the $j = 2$ line make a smaller relative contribution. Recalling that the relative populations of the j levels are nearly 1:3:5, the number of collision partners for $j = 1$ (130.49 nm) increases from $(3/9)N_{total}$ to N_{total} (a factor of 3). The number for $j = 2$ (130.22 nm) only increases from (5/9) N_{total} to N_{total} (a factor of 1.8). Consequently, the ratio of the $j = 2$ linewidth to the $j = 1$ linewidths decreases, reducing the correction for the wing of the $j = 2$ line.

The most likely source of error in the measured line shape is the presence of other absorbing species in the gas and broadening caused by collisions with species other than oxygen atoms. The residual O_2 density, at the nominal test condition, is $2 \times 10^{15} cm^{-3}$, corresponding to a background absorption of approximately 5%. The presence of scattering particles displaced from the shock tube walls during shock passage was checked by tests in pure argon. No attenuation of the beam was observed in these tests. Electrons and oxygen ions, O^+, are collision partners that compete with atomic oxygen. However, at the highest expected number density of electrons, the linewidth for electron broadening predicted by NEQAIR5 is only 4% of the measured linewidth. The broadening due to O^+ is not known, but the concentration of O^+ is essentially the same as that of free electrons. Thus, even if the ion-atom collisions are effective, they do not make a significant contribution to the broadening due to the low ion concentration.

Discussion

The shape of the $j = 1$ line of atomic oxygen has been measured out to 1200 linewidths from the line center. These appear to be the first measurements of self-broadening for this line, and they demonstrate the potential of the experimental technique for direct measurements of line shapes.

These measurements were undertaken to determine the line shape empirically and to provide data to evaluate existing line shape models, such as that used in NEQAIR5. The experimental results reported here for the $j = 1$ line show that the Lorentzian linewidth is significantly larger than the value given by NEQAIR5. However, the linewidth calculation in NEQAIR5 only includes those collision partners with oxygen atoms in the same j level as the absorber, as noted, Eq. (5).

The agreement between theory and experiment is improved substantially by including collisions with atoms in all three j levels. The $^3S^0$ excited state is connected by dipole-allowed transitions to all three j levels of the lower state. The resonance interaction between two atoms can be described by the exchange of virtual photons and is independent of the external radiation field. Therefore, collisions with oxygen atoms in all three j levels should be equally effective in broadening the line. The agreement between these measurements and the theory supports the argument that collisions with all three j levels should be included in the linewidth calculation of Eq. (5) and that N_1 is nearly equal to the total number density of oxygen atoms.

Additional experiments are planned at similar conditions but with a lower number density of oxygen. Reducing the number of oxygen atoms reduces the number of absorbing atoms and the number of collision partners. These effects will produce narrower absorption features, and higher transmission is expected between the $j = 1$ and 2 lines. The contribution from the wings of the $j = 1$ line will be reduced, and the baseline level can be measured directly. In this way, the width of the $j = 1$ line should be determined more accurately. In addition, it will be possible to determine whether the linewidth scales linearly with oxygen number density.

The experimental technique demonstrated here provides a direct measurement of the atomic line shape. Unlike curve-of-growth and effective linewidth methods, which integrate over the entire line, this technique measures absorption at individual positions on the line. Broadening by other neutral and charged particles can be determined in a similar manner if the number of perturbers can be determined and if other absorbing species either can be eliminated or corrections applied to account for them. The instrumentation developed here can also be used to measure the number density of atomic oxygen at conditions where the line shape in the wings has been determined.

Conclusions

The line shape of the $^3P_1 \rightarrow {}^3S^0$ transition of atomic oxygen at 130.49 nm has been measured out to 1200 linewidths from the line center. These measurements show the following:

1) The empirical linewidth of the $j = 1$ line is larger than that predicted by the NEQAIR5 code.

2) Agreement between theory and experiment is improved significantly by including collisions with all j levels of the ^3P ground state in the linewidth calculation.

3) This agreement is significant because accuracy of the resonance broadening model of Ref. 10 was uncertain in the line wing region.

4) The Raman-shifted excimer laser is an effective, tunable light source for absorption measurements in single-shot experiments where signal averaging is not practical.

Appendix: NEQAIR5

The NEQAIR5 code performs radiative transfer calculations for high-temperature air under conditions of thermodynamic equilibrium NEQAIR5 is based on a code first written to calculate radiative transfer by diatomic and atomic species.[20] A closed-form approximation to the Voigt profile allows computations at sufficient resolution to model emission and reabsorption for both optically thin and thick gases. The lineshape function includes contributions from Doppler, lifetime, and collisional broadening, and the collisional broadening model includes collisions with like atoms, other heavy particles, and free electrons.

NEQAIR handles the general case of radiative transfer in gases in thermodynamic nonequilibrium.[21] Excited state populations are calculated with an approximate solution to the master equations called the QSS formulation.[21,22] Master equations are written for the excited levels, including the rates of mechanisms than excite and de-excite each level. The QSS approximation assumes that the time rate of change of population in each level is much smaller than the excitation and de-excitation rates and that the QSS population can be determined by equating the excitation and de-excitation rates. In this way, excited state populations required for radiative transport calculations are determined for non-Boltzmann distributions. Excitations by collisions with electrons are much more efficient than with neutral particles, and so only electron collisions are accounted for in the current calculations. Calculations can also be performed with Boltzmann distributions instead of QSS. NEQAIR5[23] has several modifications, such as the ability to calculate radiation behind a shock wave with spatial variations; however, these capabilities are not required for these measurements.

Intensity calculations for O I lines in the near infrared are modified in two ways from that given in NEQAIR5. The three components of the 845-nm triplet are calculated individually, and some of the transition probabilities tabulated by the NBS[9] are replaced with recently calculated values.[8] Changes to the transition probabilities are small with the exception of the multiplet centered at 799 nm. The older transition probabilities for this multiplet were calculated from approximate hydrogenlike wave functions. Line intensity calculations with these theoretical A_{ul} values predict that this multiplet should be observed. Experimentally, however, this multiplet is not observed, supporting the more recently calculated values.

Absorption profiles near 130 nm are generated by NEQAIR5 as well. The QSS approximation is not required because the absorbing levels are the ground state. Unlike the lines observed in the emission measurements, however, the relevant portions of the lineshape are not dominated by Doppler broadening and cannot be calculated as reliably. Therefore, the absorption measurements are compared with these profiles to assess the accuracy of the collisional broadening model in the code.

Acknowledgments

The support for S. Meyer provided by NASA Ames Research Center through Interchange Number NCA2-723 to Stanford Uni-

versity and for E. Whiting through NAS2-14031 to Eloret Institute is gratefully acknowledged. The authors would like to thank M. Dyer and D. Huestis of the Molecular Physics Laboratory of SRI International for assistance with the Raman cell and VUV generation, C. Park and W. Huo for helpful comments, and B. Warren for operation of the EAST Facility. S. Meyer thanks D. Fletcher for many discussions during the course of this work. Finally, we note with sadness the loss of Daniel Bershader, who passed away May 30, 1995.

References

[1]Margenau, H., and Watson, W. W., "Pressure Effects of Spectral Lines," *Reviews of Modern Physics*, Vol. 8, Jan. 1936, pp. 22–53.

[2]Lochte-Holtgreven, W. (ed.), *Plasma Diagnostics*, North-Holland, Amsterdam, 1968, pp. 66–134.

[3]Griem, H. R., *Plasma Spectroscopy*, McGraw–Hill, New York, 1964, pp. 63–104.

[4]Kuhn, H. G., and Lewis, E. L., "Resonance Broadening of Spectral Lines," *Polarisation Matière et Rayonnement*, Presses Universitaires de France, Paris, 1969, pp. 341–356.

[5]Samson, J. A. R., *Techniques of Vecuum Ultraviolet Spectroscopy*, Wiley, New York, 1967, pp. 94–179.

[6]Moore, C. E., *Tables of Spectra of Hydrogen, Carbon, Nitrogen, and Oxygen Atoms*, CRC Press, Boca Raton, FL, 1993, pp. 203–222.

[7]Hilborn, R. C., "Einstein Coefficients, Cross Sections, *f* Values, Dipole Moments, and All That," *American Journal of Physics*, Vol. 50, No. 11, 1982, pp. 982–986.

[8]Hibbert, A., Biémont, E., Godefroid, M., and Vaeck, N., "E1 Transitions of Astrophysical Interest in Neutral Oxygen," *Journal of Physics B: Atomic and Molecular Physics*, Vol. 24, No. 18, 1991, pp. 3943–3958.

[9]Wiese, W. L., Smith, M. W., and Glennon, B. M., National Bureau of Standards, NSRDS-NBS 4, Vol. 1, 1966, pp. 77–82.

[10]Ali, A. W., and Griem, H. R., "Theory of Resonance Broadening of Spectral Lines by Atom-Atom Impacts," *Physical Review*, Vol. 140, No. 4A, 1965, pp. A1044–1049.

[11]Sharma, S. P., and Park, C., "Operating Characteristics of a 60 cm and a 10 cm Electric Arc-Driven Shock Tube—Part I: The Driver," *Journal of Thermophysics and Heat Transfer*, Vol. 4, No. 3, 1990, pp. 259–265.

[12]Mirels, H., "Boundary Layer Growth Effects in Shock Tubes," *Proceedings of the 8th International Shock Tube Symposium*, Chapman and Hall, London, 1971, pp. 6/1–30.

[13]Wilson, G. J., "Numerical Simulation of High Enthalpy Impulse Facilities," *Proceedings of the 20th International Symposium on Shock Waves* (Pasadena, CA) (to be published).

[14]Whiting, E. E., and Park, C., "Radiative Heating at the Stagnation Point of the AFE Vehicle," NASA TM-102829, Nov. 1990.

[15]Park, C., "Assessment of Two-Temperature Kinetic Model for Ionizing Air," *Journal of Thermophysics and Heat Transfer*, Vol. 3, No. 3, 1989, pp. 233–244.

[16]Liu, Y., Shakib, F., and Vinokur, M., "A Comparison of Internal Energy Calculation Methods for Diatomic Molecules," *Physics of Fluids A*, Vol. 2, No. 10, 1990, pp. 1884–1902.

[17]Yoshino, K., Freeman, D. E., and Parkinson, W. H., "Atlas of the Schumann-Runge Absorption Bands of O_2 in the Wavelength Region 175-205 nm," *Journal of Physical and Chemical Reference Data*, Vol. 13, No. 1, 1984, pp. 207–227.

[18]Döbele, H. F., Hörl, M., Röwekamp, M., and Reimann, B., "Detection of Atomic Oxygen by Laser-Induced Fluorescence Spectroscopy at 130 nm," *Applied Physics B*, Vol. 39, No. 2, 1986, pp. 91–95.

[19]Brink, D. J., and Proch, D., "Efficient Tunable Ultraviolet Source Based on Stimulated Raman Scattering of an Excimer-Pumped Dye Laser," *Optics Letters*, Vol. 7, No. 10, 1982, pp. 494–496.

[20]Arnold, J. O., Whiting, E. E., and Lyle, G. C., "Line-by-Line Calculation of Spectra from Diatomic Molecules and Atoms Assuming a Voigt Profile," *Journal of Quantitative Spectroscopy and Radiative Transfer*, Vol. 9, No. 6, 1969, pp. 775–798.

[21]Park, C., "Calculation of Nonequilibrium Radiation in the Flight Regimes of Aeroassisted Orbital Transfer Vehicles," *Thermal Design of Aero assisted Orbital Transfer Vehicles*, edited by H. F. Nelson, Vol. 96, Progress in Astronautics and Aeronautics, AIAA, New York, 1985, pp. 395–418.

[22]Park, C., *Nonequilibrium Hypersonic Aerothermodynamics*, Wiley, New York, 1989, pp. 89–91.

[23]Sharma, S. P., and Whiting, E. E., "Modeling of Nonequilibrium Radiation Phenomena: An Assessment," AIAA Paper 94-0253, Jan. 1994.